Engineered Science
DOI: https://dx.doi.org/10.30919/es885

Mechanistic Analysis of the Pyrolysis of Vegetable Glycerin: A Reactive Force Field – Molecular Dynamics Study

Christina Al Gemayel,[1] Joseph Zeaiter,[1,*] Soha Talih,[2, 4] Najat A. Saliba[3, 4] and Alan Shihadeh[2, 4]

Abstract

Vegetable glycerin (VG, $C_3H_8O_3$) is a triol found as an additive in food, pharmaceutical, and vaping products. Studying the pyrolysis of VG with the resulting species and their rates of formation is crucial in further understanding the underlying effects on human health. In this paper, we utilize molecular dynamics (MD) and the reactive force field (ReaxFF) to investigate VG pyrolysis. VG decomposed at a rate of activation energy Ea = 204.3 kJ/mol and pre-exponential factor A_0= 1.42E+14 s^{-1}. The main products were formaldehyde (FA), acetaldehyde (Ace), propanal (PA), acrolein (Acr), and glyoxal (GA). Both MD concentration profiles and transition state searches showed that FA, followed by AA, were the favored products. VG underwent several cracking mechanisms, with the cleavage of the hydroxyl group from the middle carbon having the lowest energy barrier ($\Delta G^{\ddagger}$ = *259.97 kJ/mol*). Longer-chained species formed via side reactions, resulting in methacrolein, crotonaldehyde, and pentanal, along with benzene and ethylbenzene intermediates. VG decomposition was found to be endothermic where the reaction rate increased with increasing system temperature. The *Ea* value for decomposition and formation reactions reached a threshold at a system density of 0.13 g/mL, while the collision factor generally increased.

Keywords: Vegetable glycerin; Pyrolysis; Kinetic model; Molecular dynamics.
Received: 17 January 2023; Revised: 07 May 2023; Accepted: 09 May 2023.
Article type: Research article.

1. Introduction

Vegetable glycerin (VG) or glycerol (1,2,3-propane-triol) is substantially used as a constituent in food flavors, personal and skin care products, and pharmaceuticals.[1] In the clean fuel industry, VG is a by-product of the transesterification reaction of triglycerides and alcohol that produces biodiesel.[2] Glycerol pyrolysis[3,4] has been regularly studied due to its ability to produce H_2 biodiesel and syngas.[5] VG is also a present in e-cigarettes, or electronic nicotine delivery systems (ENDS), that operate via the thermal decomposition of an 'e-liquid' containing propylene glycol (PG), VG, or a mixture of both, in addition to nicotine and flavors.[6]

Our previous work has studied the pyrolysis of PG via experimental and computational methods.[7,8] It has shown that toxic compounds, such as formaldehyde (FA), acetaldehyde (AA), and propanal (PA) are generated during PG pyrolysis. Jaegers *et al*. studied the pyrolysis of e-cigarette liquids containing PG and VG at low temperatures (below 200 ºC).

They presented a detailed pathway for the thermal degradation of VG in the presence of O_2, which, via hydrogen abstraction, could either form FA and AA, or acrolein (Acr), which in turn could oxidize to form acrylic acid.[9] Acrolein is a major product of glycerol decomposition and is used as an identifier of glycerol.[10] Other pathways can lead to more complex molecules such as 1(,3-dioxolan-4-yl)methanol and 1,3-dioxan-5-ol, among others, which form only due to the presence of oxygen.[9] Ooi *et al* also studied the e-cigarette emissions via a GC-MS over various PG/VG mixtures in commercially available e-cigarettes. Increasing the VG concentration in the e-liquid directly affected the emissions of toxicants, and these included AA, Acr, acetone (Ace), benzaldehyde, methacrolein, 2-propenol and aromatic compounds such as benzene, toluene, ethylbenzene, and xylene.[11] The latter compounds were formed via secondary reactions stemming from acrolein as a reactant. The C-C cracking products, ethylene and FA, underwent several

[1] *Baha and Walid Bassatne Department of Chemical Engineering and Advanced Energy, American University of Beirut, Beirut 1107 2020, Lebanon.*
[2] *Department of Mechanical Engineering, American University of Beirut, Beirut 1107 2020, Lebanon.*
[3] *Department of Chemistry, American University of Beirut, Beirut 1107 2020, Lebanon.*
[4] *Department of Psychology, Virginia Commonwealth University Center for the Study of Tobacco Products, Richmond, VA 23284, United States.*
**Email:* jz08@aub.edu.lb (J. Zeaiter)

elementary steps to form cyclic hydrocarbons, mainly benzene, which can lead to the formation of aromatic compounds. Jensen *et al*. examined the direct products and by-products of single-puff e-cigarette emissions. The e-liquid contained 1:1 by volume of PG/VG. The detected products in the aerosols included: formaldehyde hemiacetals, glycidol, enols, and aldehydes such as acrolein, lactaldehyde, glycolaldehyde, glyceraldehyde, acetaldehyde and propanal. In addition, the group presented pathways for VG decomposition initiated by H-abstraction and dehydration. C-C cleavage proceeded to give shorter-chained carbonyls such as formaldehyde, while C-H bond cleavage gave double bonds and C-O cleavage resulted in the loss of hydroxyl groups.[10,12] Wang *et al*. conducted experiments on e-liquids containing PG, VG and an equal weight mixture by vaporizing them in stainless steel reactors. At the highest temperature (318 ºC), for pure VG liquids, acrolein, acetaldehyde and formaldehyde were detected in this order of increasing microgram per milligram of VG.[13] Similarly, the same carbonyls were also detected in same order of concentration in experiments conducted by Gillman *et al*., where heating coil power was varied in five e-cigarette devices.[14] El Mubarak *et al*. developed a UHPLC-UV method for the detection of carbonyls in e-cigarette aerosols, notably FA, AA, Acr and crotonaldehyde based on previous work by Farsalinos *et al*.[15-17]

VG pyrolysis experiments were conducted at high temperatures to study the enhancement of syngas production. Valliyappan *et al*. used a tubular reactor over higher temperatures, ranging from 650 to 800 ºC over various nitrogen flow rates and packing materials. The gaseous products contained syngas (CO and H_2) at high molar concentrations, CO_2, and light hydrocarbons methane and ethane at lower molar concentrations. The increase in carrier gas (N_2) flow led to the abundance of CO and hydrocarbons over H_2.[5] Fernández *et al*. also studied the pyrolysis of VG over activated carbon in an electrical furnace with the resulting gas evaluated on a GC-TCD. The presence of hydrogen gas increased with carbonaceous catalysts, indicating that the released hydrocarbons from VG decomposition can themselves decompose to form H_2.[18] de OliveiraMaia *et al*. studied the effect of another catalyst, SBA-15 silica anchored with Schiff base complex diethylenetriamine [Ni(L1)]SBA-15 via fast pyrolysis coupled with a GC-MS. The catalyst enhanced the reaction by requiring a lower temperature and producing products at higher concentrations. The detected products, were CO_2, acrolein, formic acid (acid), propane-1-ol (alcohol), propanal, 2,3-dihydroxy- propanone.[19]

In comparison to this extensive list of experimental work available in the literature, few studies investigated the kinetic modeling of VG pyrolysis. Geng *et al*. applied density functional theory (DFT) methods to study the elementary reactions during VG pyrolysis in addition to determining the energy barriers and preferred pathways. Four possible pathways were identified, all based on dehydration and dehydrogenation. The preferred pathway was dehydration of the hydroxyl groups on the outer carbons $C_{(1)}$ and $C_{(3)}$. Then, VG becomes a 6-membered ring due to these hydroxyl groups sharing on H atom. VG then undergoes electron migration, resulting in its cracking into FA, ethanol and water via the Cyclic Grob Fragmentation mechanism.[20] Tautomerization then occurs with the ethanol resulting in the formation of AA.[21]

Zhang *et al*. employed both experimental (UPLC and TG-GC/MS) and quantum mechanical methods to study the reaction pathways of VG decomposition. Several pathways were studied, notably C—C cleavage, dehydration and dehydrogenation mechanisms. The most notable species were FA, AA, and water, and acrolein to a lesser extent. One significant intermediate was 3-hydroxypropionaldehyde.[22] Laino *et al*. also studied VG decomposition via dehydration mechanisms by employing metadynamics simulations. The preferred pathway was the formation of glycidol, which converts to 3-hydroxypropanal ultimately resulting in either Acr or FA and vinyl-alcohol (AA). The latter reaction has a lower energy barrier (35.3 kcal/mol) when compared to acrolein formation (53.9 kcal/mol).[23]

To our knowledge, no other work has employed molecular dynamics and reactive force field ReaxFF-MD for the detailed kinetic modeling of the pyrolysis of VG especially in relevance to ENDS. In this study, chemical pathways for product generation with the associated kinetic rate constants are determined, and the transition states of all possible products formation pathways are explored comprehensively.

2. Computational methods

2.1 Molecular dynamics: Reactive Force Field ReaxFF-MD

The computational tools used in this research stem from both small-scale quantum mechanics (QM) and empirical force fields (EFF) that compute system energy via interatomic potentials based on atom positions and velocity. EEFs include potentials such as harmonic, van der Waals and Coulomb interactions. While EFF do work on large systems, they only describe non-reactive or near-equilibrium systems. Therefore, this research employs reactive force fields (ReaxFF) which further include bond-order formalism, *i.e.*, the breaking and forming of bonds via chemical reactions described in Equation (1). Amsterdam Modeling Suite's ReaxFF module, initially developed by Adri van Duin, as provided by Software for Chemistry and Materials (SCM), was employed in our work[24,25]

$$BO_{ij} = BO_{ij}^{\sigma} + BO_{ij}^{\pi} + BO_{ij}^{\pi\pi} = \exp\left[p_{bo1}\left(\frac{r_{ij}}{r_o^{\sigma}}\right)^{p_{bo2}}\right] + \exp\left[p_{bo3}\left(\frac{r_{ij}}{r_o^{\pi}}\right)^{p_{bo4}}\right] + \exp\left[p_{bo5}\left(\frac{r_{ij}}{r_o^{\pi\pi}}\right)^{p_{bo6}}\right] \quad (1)$$

where the interatomic distance is denoted by r_{ij} and equilibrium bond lengths by r_o. p_{bo} (1) through (5) are empirical parameters related to the molecules involved. There

are no discontinuities through transitions between σ,π, and ππ bond character, rendering ReaxFF bond order calculations reliable for a dynamic system.

ReaxFF, and molecular dynamics in general, compute system energy in order to predict its behavior. The total energy of the system (E_{system}) is found from Equation (2).

$$E_{system} = E_{bond} + E_{over} + E_{under} + E_{\text{val}} + E_{\text{pen}} + E_{\text{tor}} + E_{conj} + E_{VdW} + E_{Coul} \quad (2)$$

E_{bond} is the bond energy found from the corrected bond order of Equation (1). To account for atom over-coordination and under-coordination, valence theory correction terms E_{over} and E_{under} are also introduced. E_{val} denotes the valence energy, while accounting for double-bonded systems sharing one atom in a valence angle via penalty energy (E_{pen}). E_{tor} stands for torsion angle energy and E_{conj} for conjugation effects. The final two terms account for non-bonded interactions: Van der Waals energy (E_{VdW}), and Coulomb interactions (E_{Coul}).

By finding system energy, MD computes the total forces on the system (F_i) in each iteration i in Equation (3), and utilizes Newton's second law to predict atoms' accelerations a_{ij} in Equation (4):

$$F_i = -\nabla E_{system\,i} \quad (3)$$

$$a_{ij} = \frac{F_i}{m_i} \quad (4)$$

where m_i is system mass at iteration i.

Atoms' velocities (v_{ij}) and positions (r_{ij}) for the next iteration j are found from equations Equations (5-6):

$$a_{ij} = \frac{d}{dt} v_{ij} \quad (5)$$

$$v_{ij} = \frac{d}{dt} r_{ij} \quad (6)$$

The cycle continues, where energy is again found for the new position, thus force is predicted, giving acceleration, and this continues until the system finishes the set of iterations and reaches its final state.

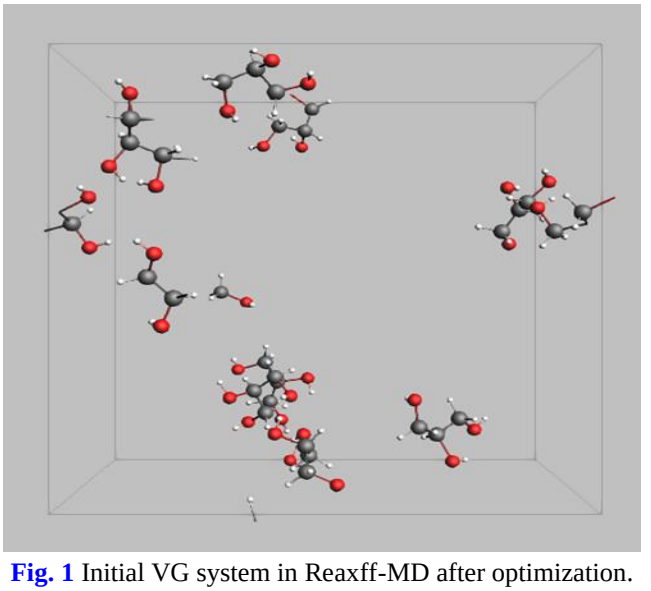

Fig. 1 Initial VG system in Reaxff-MD after optimization.

2.1.1 Initial system

A simulation box of 23*23*23Å^3 box was created using the Packmol package,[26] with 10 randomly generated VG molecules inside, yielding a density of around 0.13 g/mL. This system must be geometrically optimized, *i.e.*, reach a global minimum on the potential energy surface, before it can be used for further simulations. The first step of system optimization entailed a microcanonical ensemble (NVE: fixed Number-Volume-Energy) run at 5 K for 10ps where energy reached a minimum. The subsequent configuration was then subjected to a canonical ensemble with a Berendsen thermostat (NVT: fixed Number-Volume-Temperature) of 100 fs damping constant at 1000 K for 10 ps. This ensures equilibration of all system energies. Therefore, the resulting system was used as an initial configuration for all the following simulations. The force field applied in all computations was the CHO-2016.ff. A time step of 0.1 fs/iteration was used.

2.1.2 Annealing simulations

The first batch of simulations conducted were the annealing runs, where the initial system was subjected to a temperature ramp until it reaches the desired final temperature. To elaborate, the equilibrated system exhibited a 500 ps temperature increase from 1000 K to the final maximum temperature T_{Max}, where it will remain for another 500 ps. The chosen T_{Max} ranged from 3000 K to 4000 K at a 250 K interval. Each chosen T_{Max} simulation was run in triplicates and the results were averaged. The NVT method was applied throughout. Annealing simulations help study system behavior, reactions involved, products formed and concentration profiles. High temperatures are commonly employed in ReaxFF-MD simulations to obtain results in real-time as they do not affect kinetic rate constants (K) since the relationship between ln(K) and 1/T is generally linear.[27-34]

2.1.3 Isothermal simulations

In the second batch, the initial system was subjected to an isothermal temperature for 100 ps, ranging between 2000 K to 4000 K at 250 K intervals. Similar to the annealing simulations, triplicates were run for each isothermal temperature using the canonical ensemble, and the results averaged. The purpose of these runs is to study reaction kinetics.

2.2 Transition state search

The other computations in the research are derived from points found on the potential energy surface (PES). Also known as an energy profile, PES is essentially a potential function that relates atomic and molecular collisions to inter-nuclear coordinates, *i.e.*, to geometry. This stems from the theory that every single system geometry has a unique energy associated to it. PES plots energy versus two geometry parameters, usually bond lengths and bong angles. From a PES, one can derive minimum energy points at valley bottoms, which is useful in initial system geometry optimization where stable atoms seek the lowest energy path. One can also derive transition states at saddle points that indicate the transition

from a reactant to a product, *i.e.*, the reaction activation energy.[35]

To study elementary reactions and possible pathways, a potential energy plot was built via ReaxAMS, which combines QM theory with reactive force field. Initial and final systems (i.e. reactant and products) are required for this plot. Firstly, these two systems were geometrically optimized to reach a minimum on the PES and to improve bond lengths and angles via the universal force field (UFF). Secondly, the CHO-2016.ff was applied to minimize the energy on the specified molecule. To plot the PES, the nudged elastic band (NEB) functionality was employed: it takes the initial system and predicts the energy path leading to the final system by optimizing the intermediate systems, or images. The lowest energy possible from one image to the next was found by adding spring forces along the band between images, resulting in the potential perpendicular to the band projected out, predicting the next image. From the energy path found, transition state search was applied, which helped in assessing preferred reaction pathways and energy barriers.

3. Results and discussion

3.1 Product distribution from ReaxFF-MD

To explore the cracking mechanisms of VG pyrolysis, the Reaction Event Detection tool in ReaxFF's ChemTraYzer plug-in was employed. The major pathways observed are presented in Fig. 2.

Common observed species are molecules with unpaired electrons, as elementary reactions are presented in ChemTraYzer. The main cracking products are the following radical intermediates:

- $C_3H_7O_2$ from the loss of –OH bonds (or dehydration)
- $C_2H_5O_2$ from C—C bond cleavage
- CH_3O from C—C bond cleavage
- $C_3H_7O_3$ from H abstraction

Cracking products can undergo further decomposition to obtain secondary products as shown in Fig. 3. Despite having unpaired electrons, the obtained species are key in understanding the reactions taking place on the elementary and molecular level. These free radicals from ChemTraYzer will be referred to in the text as the aldehyde species they are associated with based on their bonds.

These detected species are in accordance to the aldehydes presented in VG pyrolysis experiments in the literature.[9-11,13-15] Further discussions on the reaction mechanisms are presented in Section 3.4, where transition states, preferred pathways and energy barriers are discussed.

Subsequently, every species' number (N) versus iteration. xy file was extracted. Fig. 4 shows the averaged N (over triplicates) versus time of all the species at T_{Max} of 3000 K. VG began decomposing at a temperature of around 2000 K, prior to reaching the isothermal temperature T_{Max}. However, it exhibited a much sharper decomposition as it approaches T_{Max}, and decomposed fully before the system reached the isothermal mode.

The number of VG molecules are plotted in Fig. 5 against the major decomposition products: FA and AA, and its subsequent product GA, PA and Acr, and H_2O and H_2 molecules.

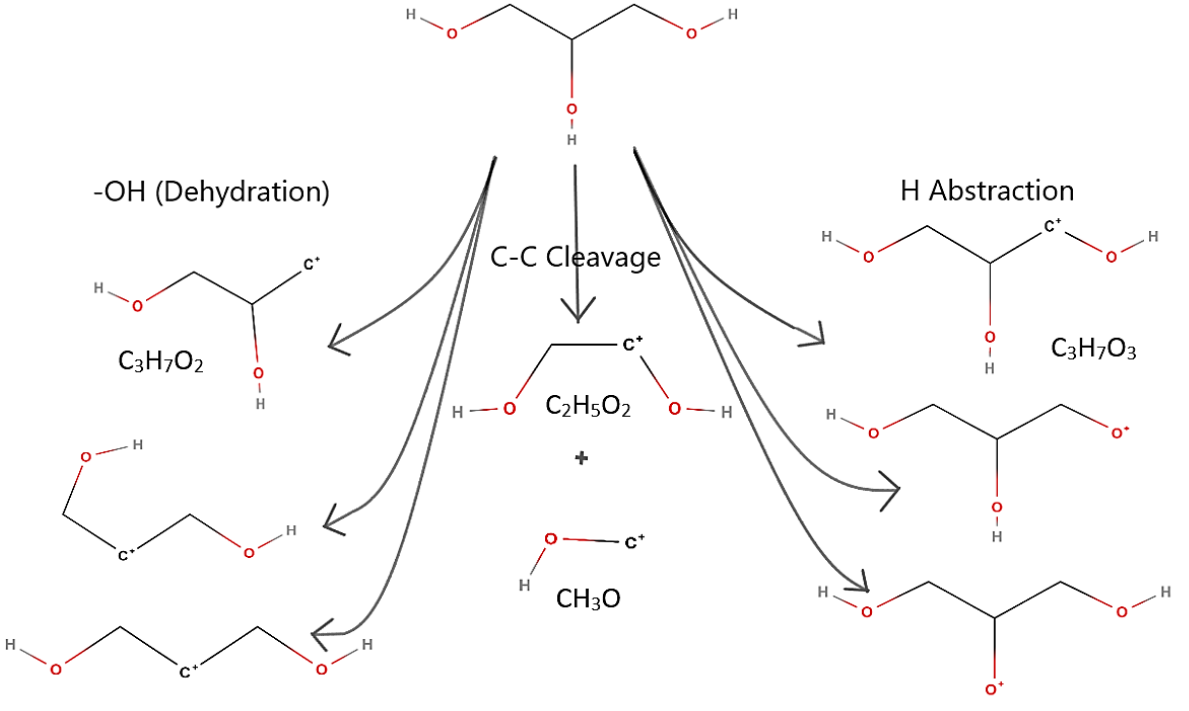

Fig. 2 VG Decomposition products from ChemTraYzer. Three main pathways are possible: loss of OH group, carbon-carbon bond cleavage, and loss of H atom.

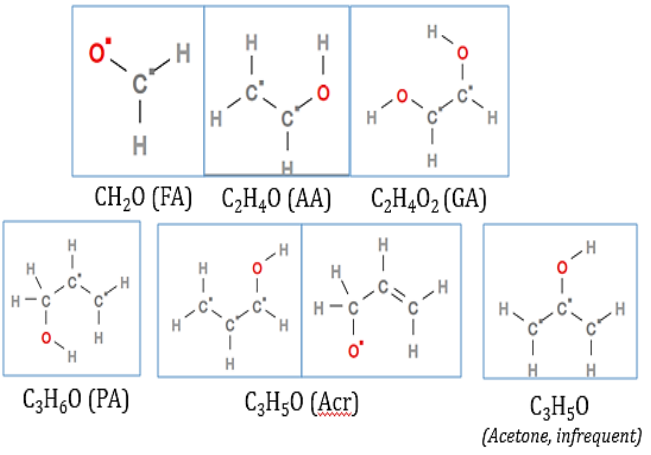

Fig. 3 Notable species obtained from ChemTraYzer.

Formaldehyde formed at the highest concentration and kept increasing even after VG was fully consumed due to several cracking reactions. It was later consumed as the simulation proceeded. Acetaldehyde, glyoxal, propanal and acrolein formed at lower concentrations when compared to formaldehyde, and decomposed towards the end of the simulation. $C_3H_7O_3$ and $C_3H_7O_2$ formed earlier in the simulation, but underwent further reactions and were converted to other, more significant, secondary products. Water and hydrogen were formed in abundance, denoting that dehydration and dehydrogenation are the reactions predominantly occurring. From Fig. 5(a), FA and AA form more frequently and at higher concentrations, noting that they are the dominant products. In fact, literature has shown that FA and AA formation are the preferred pathways based on DFT calculations on Gibbs free energy.[21,23]

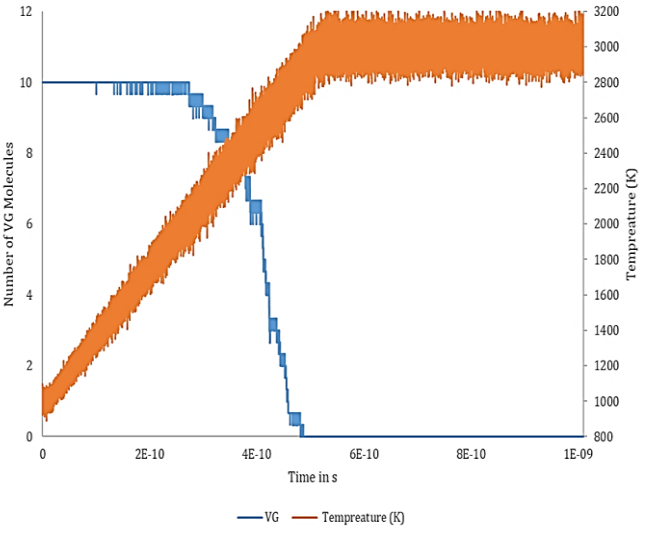

Fig. 4 VG Decomposition throughout simulation time with temperature profile. Isothermal temperature = 3000 K.

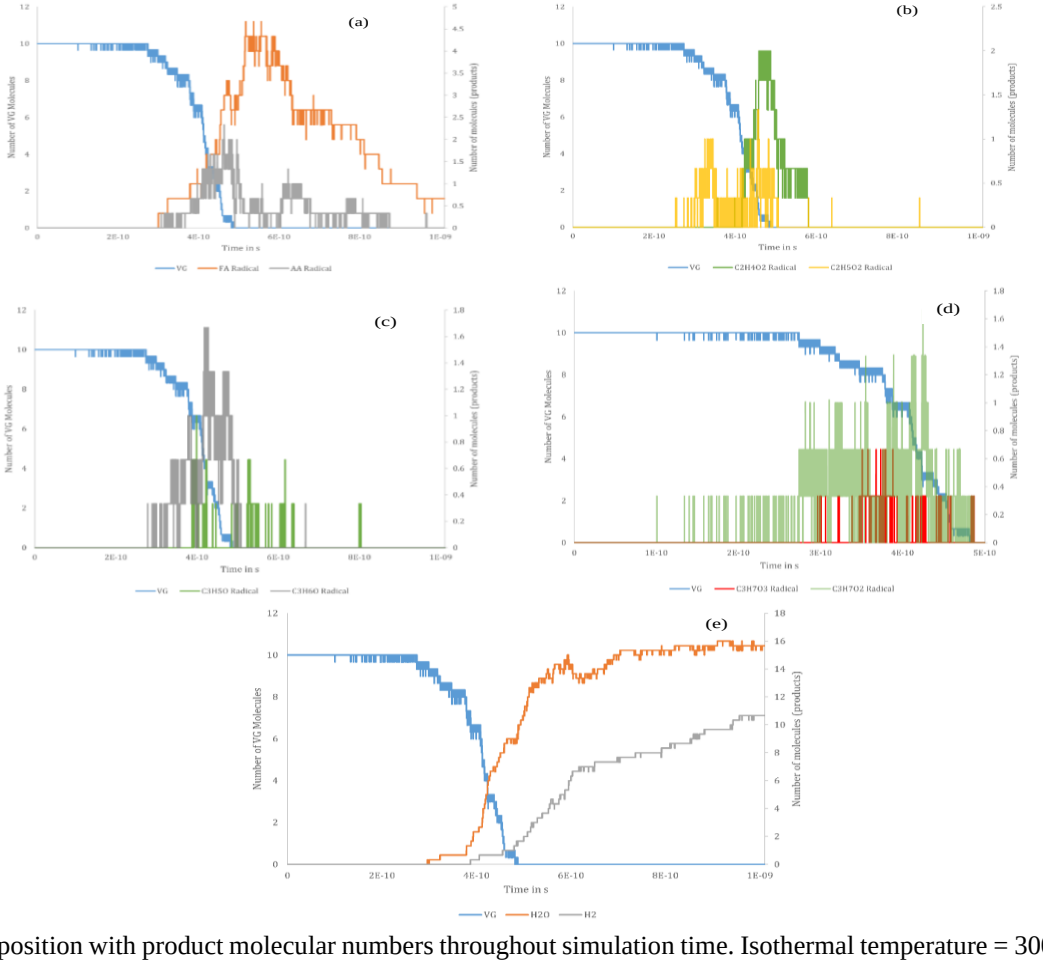

Fig. 5 VG Decomposition with product molecular numbers throughout simulation time. Isothermal temperature = 3000 K (a) FA and AA (b) $C_2H_5O_2$ and GA (c) PA and Acr (d) major intermediates $C_3H_7O_2$ $C_3H_7O_3$ (e) H_2O and H_2 molecules.

3.2 Kinetic analysis of VG Pyrolysis

3.2.1 VG overall decomposition

From isothermal ReaxFF-MD simulations, the overall decomposition of VG can be found, over the temperature range of 2000 K to 4000 K, based on the following in Equation (7),

$$VG \xrightarrow{k_{Decomposition}} Products \quad (7)$$

Where $k_{Decomposition}$ at every temperature is found from Equation (8):

$$lnN - lnN_0 = k_{Decomposition} * t \quad (8)$$

over every time (t) increment. LnN versus time was plotted linearly to obtain $k_{Decomposition}$ as a slope. Arrhenius parameters were then found by plotting the k-values over temperature as $\ln(k_{Decomposition})$ versus $\frac{1}{T}$ from the Arrhenius equation (Equation (9)),

$$k_{Decomposition} = A_0 * \exp\left(\frac{-E_a}{RT}\right) \quad (9)$$

Then the logarithmic form was applied to give Equation (10),

$$\ln(k_{Decomposition}) = \ln(A_0) + \frac{-E_a}{RT} \quad (10)$$

Where the slope of the linear plot is $\frac{-E_a}{R}$ and the y-intercept is $\ln(A_0)$. An Ea of 204.3 kJ/mol and A_0 of 1.42E+14 s^{-1} were obtained as seen in Fig. 6.

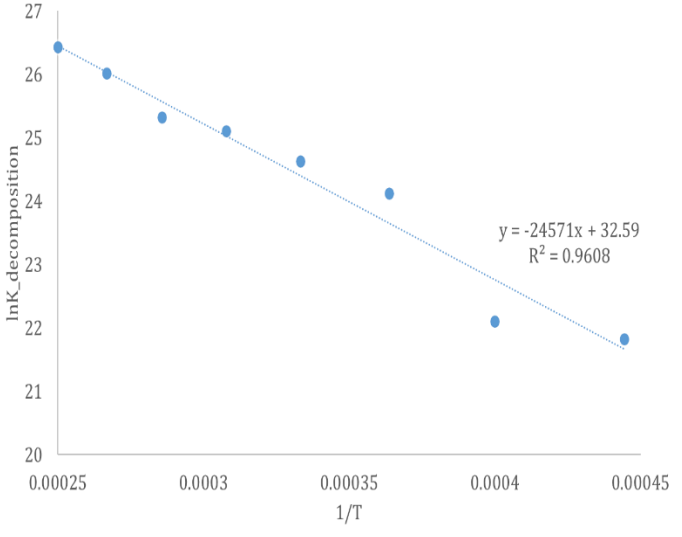

Fig. 6 Natural logarithm plot of k-value of VG decomposition versus inverse temperature (K^{-1}).

3.2.2 Product formation

The rates of formation of the notable species, or aldehydes, from ReaxFF-MD were found based on Equation (11),

$$VG \xrightarrow{k_{Formation\ X}} Aldehyde\ X \quad (11)$$

The number of molecules N of every relevant species was converted to concentration using Equation (12),

$$Concentration\left(\frac{mol}{m^3}\right) = \frac{N}{Avogardo'sNumber * system\ volume\ in\ m^3} = \frac{N}{6.022*10^{23}mol^{-1}*(2.3*10^{-9})^3 m^3} \quad (12)$$

Where from Equation (13) the change in aldehyde concentration over every time increment is obtained from its rate constant of formation and the concentration of VG,

$$\frac{d[Aldehyde\ X]_{predicted}}{dt} = k_{Formation\ X} * [VG]_{predicted\ t} \quad (13)$$

$k_{formation\ X}$ is a variable that is optimized by minimizing the RMSE between [Aldehyde X]$_{predicted}$ and the actual concentration [Aldehyde X]$_{actual}$ from ReaxFF-MD simulations. $[VG]_{predicted\ t}$ was obtained from Equation (14),

$$\frac{d[VG]_{predicted\ t}}{dt} = -k_{Decomposition} * [VG]_{predicted\ t} \quad (14)$$

where $k_{Decomposition}$ is obtained from Equation (9).

For instance, the rate of formation of FA at 3000K was obtained by minimizing the error between two data sets: (1) [FA] found from ReaxFF-MD and (2) predicted [FA] based on Equation (13). These are shown in Fig. 7.

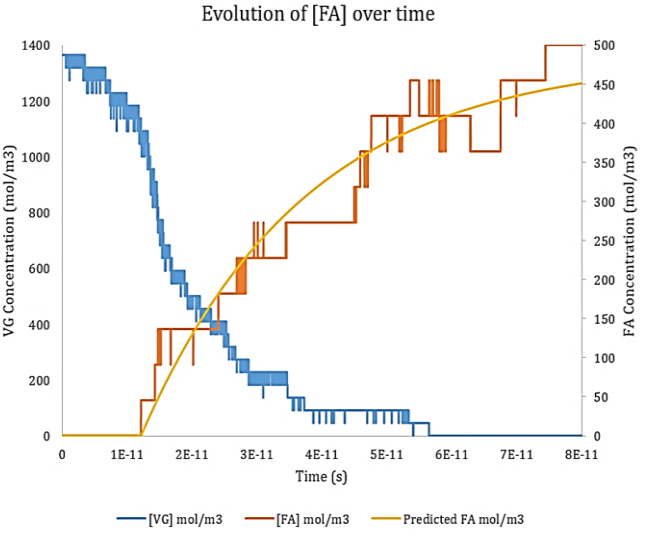

Fig. 7 Evolution of FA over simulation time at 3000 K from ReaxFF-MD and variable optimization along with VG decomposition.

It is important to note that all reactions were performed as per equation (3), except the formation of Acrolein. As seen in Fig. 5(c), Acr disappears in short 'spikes' and does not follow a trend where it increases logarithmically over time, similar to the other species. The formation rate constant $Rate_{Acr\ Formation}$ is obtained for the time when Acr forms and disappears as shown in Equations (15-16).[8]

$$Rate_{Acr\ Formation} = \frac{\Delta[Acr]}{\Delta t} = \frac{[Acr]_{final} - [Acr]_{initial}}{t_{final} - t_{initial}} \quad (15)$$

$$k_{Acr\ Formation} = -\frac{Rate_{Acr\ Formation}}{[VG]_{at\ t_{final}}} \quad (16)$$

The Arrhenius constants for the rates of formation of aldehydes are obtained from Equation (9) and summarized in Table 1. The linear fitting plots for the k-values of formation are found in the Supplementary data.

3.3 Sensitivity analysis

3.3.1 Temperature sensitivity

The effect of temperature on the overall decomposition of VG is studied. VG started decomposing at 3000 K. As

temperatures increased, reaction rates sped up and therefore, VG decomposed faster. VG decomposition is thus an endothermic reaction, requiring temperature and heat to undergo thermal decomposition. Nevertheless, as seen in Fig. 8 the same profiles are exhibited showing that VG decomposition is of first-order.

Table 1. Activation energy(J/mol) and pre-exponential factor (1/s) values of carbonyl formation from ReaxFF-MD and linear fitting.

Product	k_Formation		R^2
	Ea (kJ/mol)	A_0 (1/s)	value
FA	256.7	6.67E+14	0.9998
AA	225.9	1.21E+14	0.8605
GA	142.9	3.24E+12	0.9994
PA	302.9	1.91E+15	0.9951
Acr	299.7	7.51E+14	0.8434

Note that the R^2 value for Acr is a result of the spikes that have made kinetic modeling less than ideal.

To study the effect on product formation, data was collected at 30ps in every set of isothermal simulations from 2750 K to 4000 K (where the number of molecules was averaged over the triplicates at each isothermal temperature). The number of molecules for the relevant species is noted in Table 2. For 2750 K and 3000 K, VG has not yet fully decomposed at 30ps, while it did beyond 3250 K. The FA slowly increased with temperature, reaching a threshold at 3750 K, after which it started to be consumed sooner, as expected from Fig. 5(a). The AA exhibited faster decomposition with the increase in isothermal temperatures. GA formed sooner as temperature increased to 3250 K, after which it underwent side reactions to reach a full decomposition at 4000 K beyond 30ps. PA and Acr also exhibited similar trends, with the former starting 'early' decomposition at 3250 K, and the latter at 3500 K.

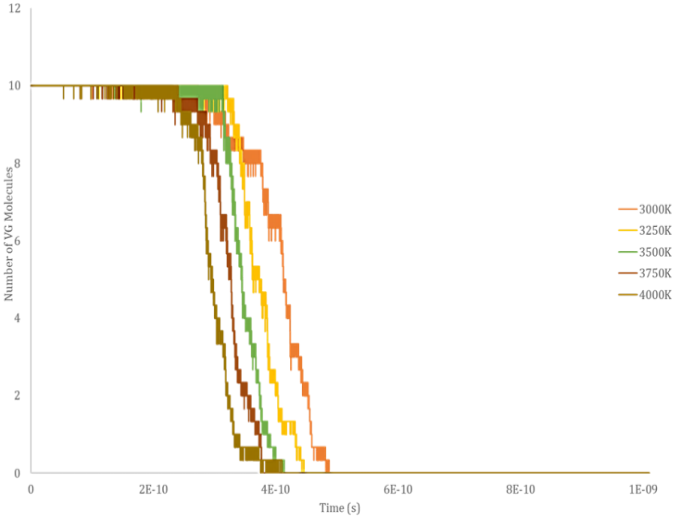

Fig. 8 VG decomposition throughout simulation time over different temperatures.

Table 2. Notable products' molecular number (N) as observed at the end of 30 ps isothermal simulations.

T (K)	FA	AA	GA	PA	Acr
2750	2.0	2.0	0.0	1.0	0.7
3000	1.7	1.3	0.7	1.3	1.0
3250	2.0	1.0	1.0	1.0	1.0
3500	2.7	0.7	0.3	0.7	0.3
3750	3.7	0.0	0.3	0.0	0.0
4000	3.0	0.0	0.0	0.0	0.0

3.3.2 Density sensitivity

The effect of density was studied in this work. VG molecules were placed in a box of varying dimensions presented in Table 3:

Table 3. The various system densities used.

Simulation label	Box dimensions	Density g/mL
ρ_1	50*50*50 Å^3	0.01
ρ_2	23*23*23 Å^3	0.13
ρ_3	19*19*19 Å^3	0.22

Annealing simulations were run to study the effect on pathways and concentration profiles while isothermal simulations were conducted to study the effect on reaction kinetics.

ρ_1 simulations had the largest box volume and thus collisions were fewest, resulting in less reactions and a slow decomposition of VG. On the other hand, ρ_2 runs, which were 10 times denser than ρ_1, had higher collision frequencies and therefore a sharper decrease of VG. They were close in VG decomposition to ρ_3 simulations as the latter were only twice denser than ρ_2. Attempting to create a denser box was not feasible as the atoms became too close to conduct proper computations. It can be concluded that the system has reached a certain threshold density at ρ_2 where results are similar beyond it and can no longer compute after ρ_3. To validate this assumption, further isothermal runs were conducted, and the same methodology was used to calculate the Arrhenius parameters for $k_{Decomposition}$ for VG and $k_{Formation}$ for the aldehyde products.

Table 4. Activation energy (J/mol) values of carbonyl formation from ReaxFF-MD over various densities.

Ea	ρ_1	ρ_2	ρ_3
VG Decomposition	169.6	204.3	222.1
FA Formation	198.3	256.7	244.3
AA Formation	168.7	225.9	225.1
GA Formation	145.4	142.9	144.7
PA Formation	236.5	302.9	295.1
Acr Formation	303.2	299.7	296.4

The activation energies are presented in Table 4. For VG decomposition, as system density increased from ρ_1 to ρ_2, activation energies increased. Furthermore, and as illustrated in Fig. 9, VG decomposition exhibited comparable evolution

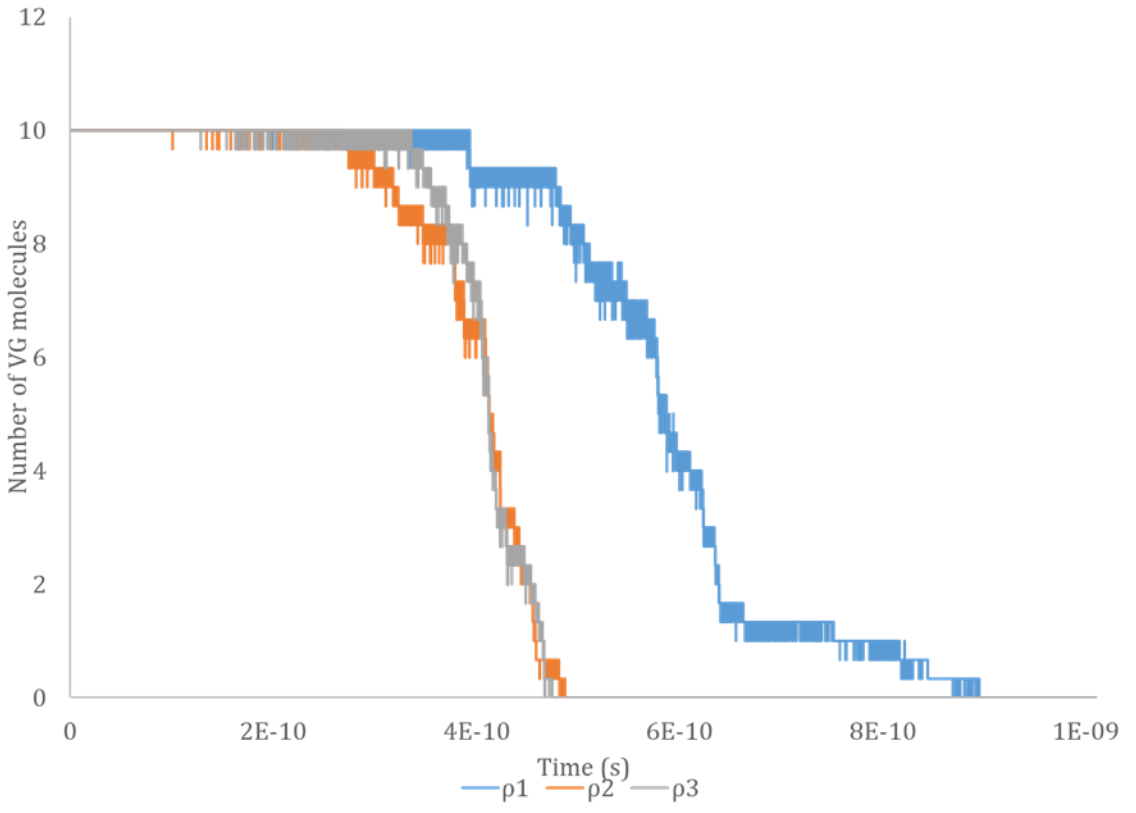

Fig. 9 VG decomposition throughout simulation time over different densities.

under ρ_2 and ρ_3 and a less sharp decrease in ρ_1. This behavior also appeared in FA, AA and PA decomposition. GA exhibited similar activation energies throughout all densities, which could be due to the fact that it requires less energy-intensive elementary reactions to be formed, as will be further discussed in Section 3.4. Similarly, Acr exhibited approximately close values for Ea across the three densities.

Denser system exhibited higher collision factors, as shown in the A_0 values of ρ_1 and ρ_2 in Table 5. Values under ρ_2 and ρ_3 were generally of the same order, indicating that these two densities have reached a certain threshold. For GA and Acr, Ao values followed the same trend where the values increase within the same order across the increasing densities.

Table 5. Pre-exponential factor (1/s) values of carbonyl formation from ReaxFF-MD over various densities.

Ao	ρ_1	ρ_2	ρ_3
VG Decomposition	1.04E+13	1.42E+14	4.07E+14
FA Formation	1.11E+13	6.67E+14	4.84E+14
AA Formation	3.14E+12	1.21E+14	1.70E+14
GA Formation	1.17E+12	3.24E+12	6.16E+12
PA Formation	3.58E+13	1.91E+15	1.28E+15
Acr Formation	1.49E+14	7.51E+14	8.55E+14

3.4 Cracking and production mechanisms: Elementary reactions

The ChemTraYzer tool was employed to closely study the elementary steps of VG pyrolysis. Results from annealing and isothermal runs were observed, over all triplicates and temperatures, to obtain a holistic pathway from VG to the aldehydes in question. The pathways were organized as follows: (1) cracking pathways for VG, (2) formation pathways for aldehydes. Every reaction was studied on ReaxAMS's NEB method to obtain transition states and thus the standard Gibbs free energy of activation at 298.15 K ($\Delta^{\ddagger}G^{o}$ or simplified to $\Delta G^{\ddagger}$ in this work). If the NEB method was unable to converge to a pathway, the PES scan method, also offered by ReaxAMS, was applied. Rather than building images between the initial and final image, the PES scan takes in initial and final bond orders, lengths and angles to predict the pathway.

3.4.1 VG elementary reactions

Eight possible pathways were observed for VG decomposition, based on which bonds undergo cleavage. These are presented in Fig. 10 and Fig. 11. In ReaxAMS, the standard Gibbs free energies of each of the reactant, product and transition state were found and plotted, as seen in Fig. 12, where the pathways are overlaid to note the energy barriers. Two types of reactions were observed: direct cracking of VG → products (Pathways A to E), and reactions where VG reacted with an H ion or an OH group (Pathways F, G and H). The changes in Gibbs free energy of activation, from reactant to TS, $\Delta G^{\ddagger}$ in kJ/mol, are listed in Table 6.

Pathway A adopts carbon-carbon cleavage, resulting in $C_2H_5O_2$ and CH_3 intermediates. VG underwent H abstraction, or loss of an H atom, in pathway B resulting in the $C_3H_7O_3$

($C_{(1)}^+$) intermediate. Pathways C, D and E detail the loss of an –OH group, based on which carbon underwent C—OH cleavage, or dehydration. In addition, the orientation of the remaining –OH bonds in the product is also observed due to the effect of bond angles on bond energy.[36] Bond energy plays a role in how much energy is required to break a bond. This indirectly affects the enthalpy change of the system (ΔH), thus the Gibbs free energy (ΔG = ΔH – TΔS). The dehydration mechanism E was similarly mentioned by Geng *et al.* on VG pyrolysis, where either $C_{(2)}$ lost an –OH bond.[21] Further dehydration on the $C_3H_7O_3$ ($C_{(2)}^+$) intermediate resulted in the Acr molecule, while it can undergo further reactions and C—C cleavage to form FA and AA.

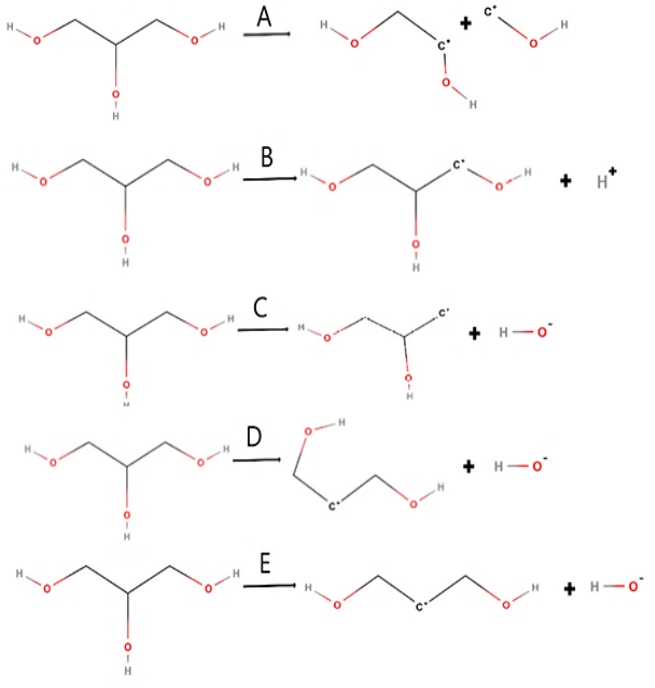

Fig. 10 Direct VG cracking pathways. VG undergoes C-C cleavage (pathway A), dehydrogenation (pathway B) and dehydration (pathways C, D and E).

VG can form water molecules via pathways F, G and H. In pathway F, VG underwent C—OH cleavage, and the resulting –OH hydroxyl radical bonded with a free H atom. As a result a $C_3H_7O_2$ intermediate is formed. On the other hand, in pathways G and H, one of the hydroxyl groups lost an H atom, which in return bonded with the free –OH. This hydroxyl radical could be a product from the occurring pathways C, D and E as they undergo –OH abstraction. The difference between F and G lies in the location of the original hydroxyl group. Therefore, two possible $C_3H_7O_3$ intermediate radicals are formed. Pathway G was also highlighted in the works of Geng *et al.*, where the resulting $C_3H_7O_3$ ultimately decomposed via dehydration into FA and AA in a process known as alkaline-pinacol rearrangement/retro-aldol fragmentation. No transition states were found by the group.[21] The cracking reactions presented in our work are in accordance to the one presented in Jaegers *et al.*.[9] H-abstraction, followed by C—O cleavage, resulted in (1) the formation or FA and AA from 1-hydroxypropan-2-ol (the intermediate formed in pathway C), and (2) acrolein formation from 3-hydroxypropanal (the intermediate formed in pathway E). In addition, C—H cleavage on the $C_3H_7O_3$ radical resulted in 2,3-dihydroxypropanal and 1,3-dihydroxypropan-2-one, similar to the intermediates formed in pathways G and H, respectively.

Table 6. Gibbs free energy barriers for VG reactions at 298.15K.

Pathway	ΔG‡ (kJ/mol)
A	501.9
B	340.4
C	313.6
D	271.6
E	260
F	11.8
G	28.2
H	19.3

Pathway E, in which VG underwent cleavage between $C_{(2)}$ and OH (dehydration), has the lowest energy barrier for the cracking reactions with $\Delta G^{\ddagger}$ = 259.97 kJ/mol, resulting in a $C_3H_7O_2$ intermediate. This is in accordance to the reaction presented by Laino *et al.* where VG decomposed into 3-hydroxypropanal with glycidol as an intermediate. The $C_3H_7O_2$ resulting from pathway E can be considered as a 3-hydroxypropanal radical as it has a hydroxyl group on $C_{(1)}$ rather than the double bond $C_{(1)}$=O was present. The energy barrier presented by Laino *et al.* was 207.108 kJ/mol at 800 K, close to our value 243.54 kJ/mol (recomputed at 800 K).[23] In addition, Geng *et al.* studied a similar pathway where VG undergoes dehydration on the $C_{(2)}$, resulting in a product similar to the one formed in pathway E, but with a double bond on $C_{(2)}$, with a Gibbs energy barrier of 288.59 kJ/mol at 800K.[21] Our computed change in Gibbs free energy lies in between these two references.

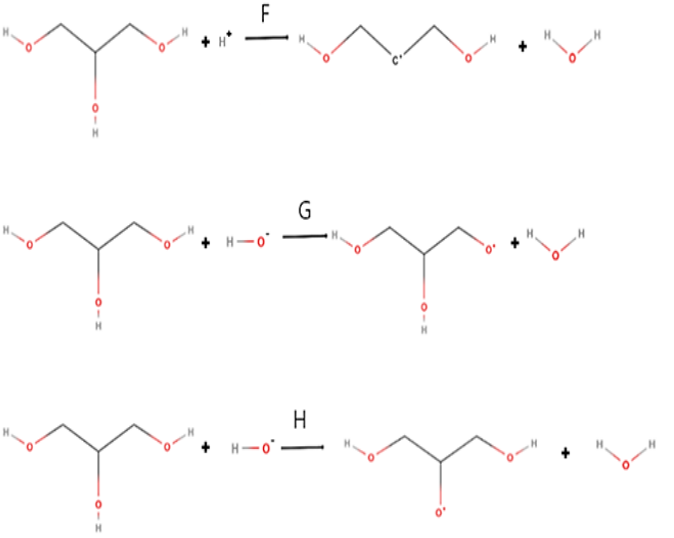

Fig. 11 VG Reactions with free H ion and OH group to form water molecule.

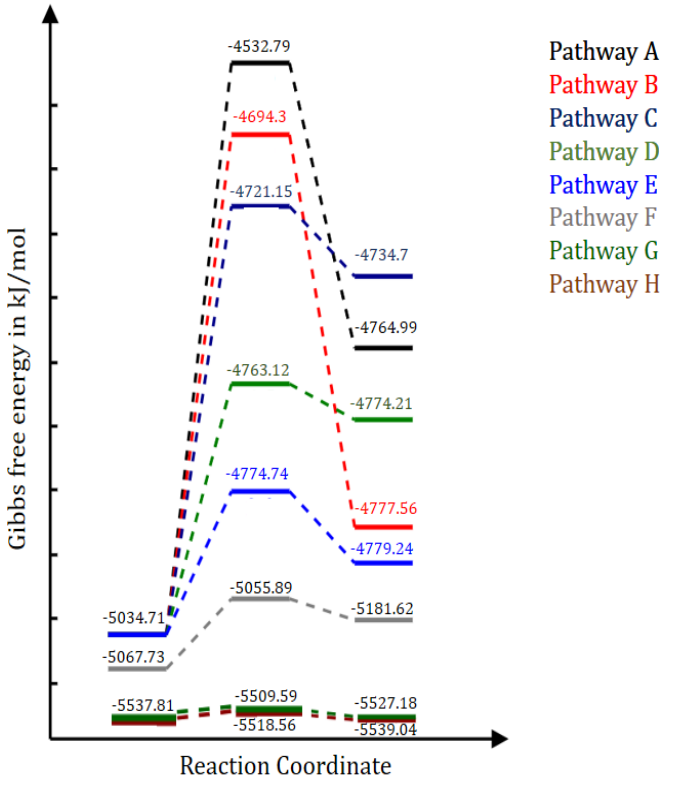

Fig. 12 Gibbs free energy plots of VG reactions at 298.15K.

In addition, Geng *et al*. also studied a pathway similar to pathway D, where the resulting intermediate hydroxyl groups on $C_{(1)}$ and $C_{(3)}$ are on opposite sides, with an energy barrier of 269.47 kJ/mol at 800 K, which is close to our computed value of 244.37 kJ/mol at the same temperature. It is important to note that the energy barrier for pathway D is lower than the one they proposed for pathway E, which is the opposite case in our findings. Nonetheless, the free energy barriers' difference between our proposed pathways D and E is only 0.83 kJ/mol at 800K, indicating that the orientation of the hydroxyl groups does not play a significant role in defining the rate-limiting step.

Pathways F, G and H (bimolecular reactions) exhibit energy barriers lower than the aforementioned unimolecular reactions (pathways A to E) by at least one order of magnitude. This low barrier is due to the O—H bond cleavage, which is then compensated by another O—H bond formation. Thus, the barrier heights of pathways A-E are not compared against those of pathways F-H. However, the relevant products are observed. Notably, G and H form a common radical present in MD simulations: $C_3H_7O_3$, which in turn decomposed to $C_2H_4O_2$ and CH_3O as will be presented in the Section 3.4.2.

3.4.2 Formation mechanisms for main products

$C_2H_5O_2$ formed mainly from the direct cracking of PG as seen in pathway A. It proceeded to undergo C—OH cleavage, resulting in AA (pathway AA—1). In addition, AA can form from the $C_3H_7O_2$ radicals via C—C cleavage, as seen in pathways AA—2 a, b and c, depending on which $C_3H_7O_2$ is the reactant. Finally, AA can also form via AA—3, where $C_3H_6O_2$ underwent C—C cleavage, resulting in FA too, as shown in Fig.13 that summarizes all AA reactions. All associated Gibbs plots are found in Fig. 14.

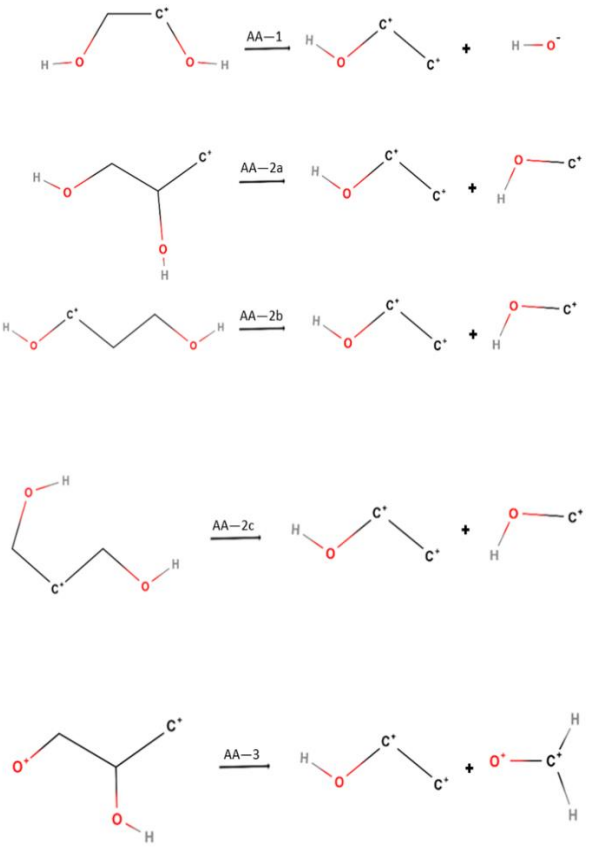

Fig. 13 AA formation from different reactants.

Reaction AA—2a started with an isomer of the 3-hydroxypropanal radical, and had an energy barrier of 178.65 kJ/mol at 298.15 K. It is similar to 3-hydroxypropanal conversion reaction into FA and vinyl-alcohol (or AA) as presented by Laino *et al*. The latter found an energy barrier of 147.7 kJ/mol.[23] In order to compare our findings with the literature, we re-computed the energy barrier at 800K for Reaction AA—2a and this resulted in an energy barrier of 160.51 kJ/mol with an absolute error of 12.81 kJ/mol.

C_3H_6O, or PA, can be obtained from three pathways, all resulting from the C—OH cleavage of the $C_3H_7O_2$ free radicals, as seen in Fig. 15. The associated Gibbs free energy plots are presented in Fig. 16.

PA underwent carbon-carbon cleavage between the middle C and the outer C bonded with OH in Fig. 17. The CH_3O intermediate formed, which, via pathways FA—1, 2 and 3, underwent dehydrogenation and resulted in CH_2O (FA) in Fig. 18. The associated Gibbs energy plots are found in Fig. 19.

The $C_3H_7O_2$ intermediate resulting from pathway E underwent H transfer from $C_{(2)}$ to $C_{(1)}$. It can then further decompose into either: (1) C_3H_6O via pathway C_3H_6O—2 (dehydration), which can undergo C—C cleavage to give CH_3O, later forming FA as in Fig. 18, and (2) AA and CH_3O radical via pathway AA—2b (Fig. 13), where CH_3O can also

lead to FA formation. Thus FA, and less notably AA, are the preferred products in VG thermal decomposition. This is in accordance to both Geng *et al*. and Laino *et al*. results, where the formation of FA and AA is the preferred mechanism over acrolein formation.[21,23]

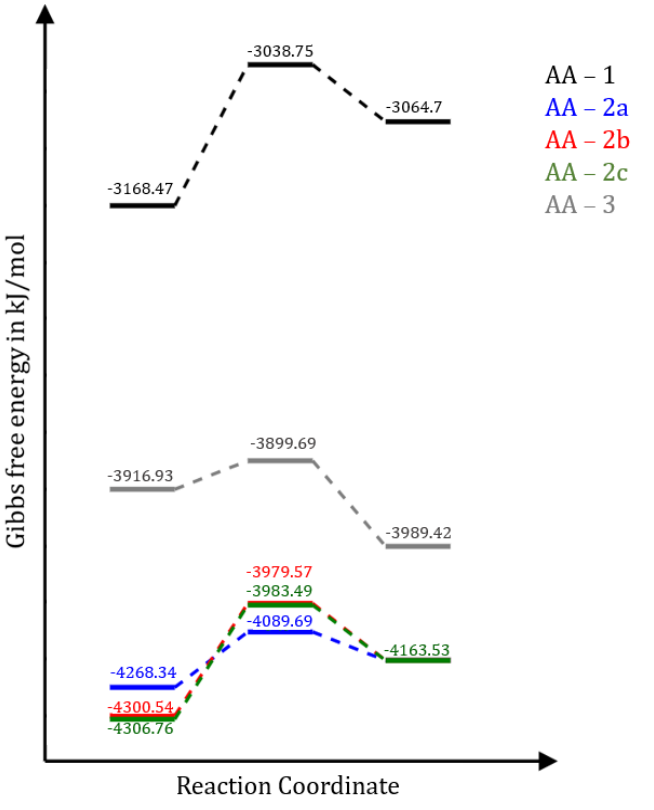

Fig. 14 Gibbs free energy plots of AA formation reactions at 298.15K.

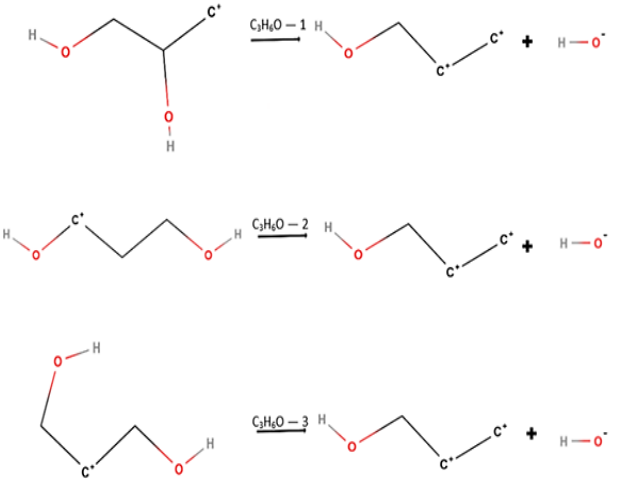

Fig. 15 C_3H_6O Formation from different $C_3H_7O_2$ species.

The $C_3H_6O_2$ intermediate formed from the C—OH cleavage in $C_3H_7O_3$ radical as shown in Fig. 20. It then proceeded to further lose a hydroxyl group, forming C_3H_5O (Figs. 21-22), which, based on its free electrons, is associated to the Acr molecule (pathway C_3H_5O—1). Pathway C_3H_5O—2, on the other hand, results from $C_{(1)}$—H breakage in C_3H_6O or PA.

C_3H_5O — 1 reaction is similar to the one presented by Laino *et al*. on the formation of acrolein from 3-hydroxypropanal, where the energy barrier was found to be 225.52 kJ/mol, close to our computed value of 239.82 kJ/mol at 800K.[23]

$C_2H_4O_2$, referred to as GA, formed from two pathways in Fig. 23, based on which O molecule originally underwent H abstraction (Pathways G and H) in VG cracking. Both entail the C—C cleavage between $C_{(1)}$ and $C_{(2)}$, in $C_3H_7O_3$,where $C_{(1)}$ is bonded to the –OH radical. H is then transferred from C to the O^+ radical.

Despite the proximity in the energies of the initial system, GA—2 required less energy to reach a transition state as shown in Fig. 24.

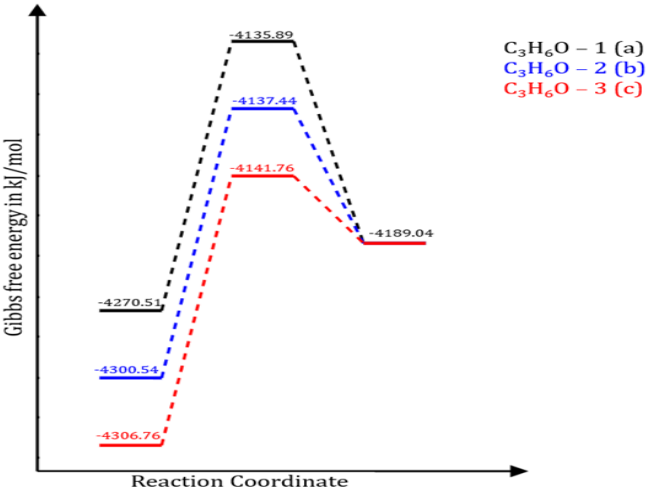

Fig. 16 Gibbs free energy plots of C_3H_6O formation reactions at 298.15K.

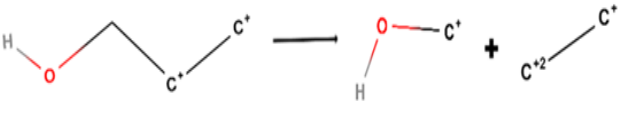

Fig. 17 CH_3O formation from PA.

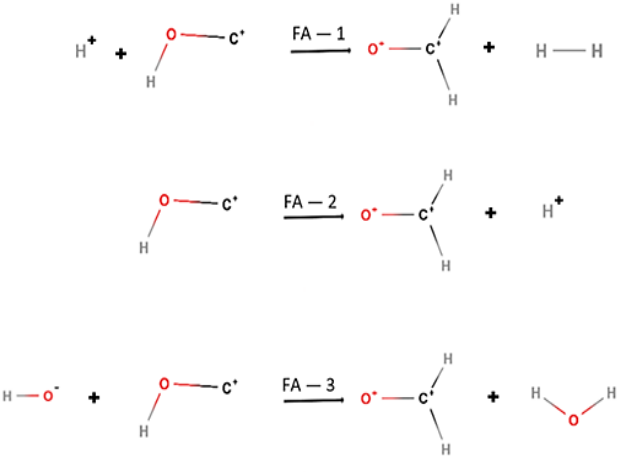

Fig. 18 FA formation from CH_3O.

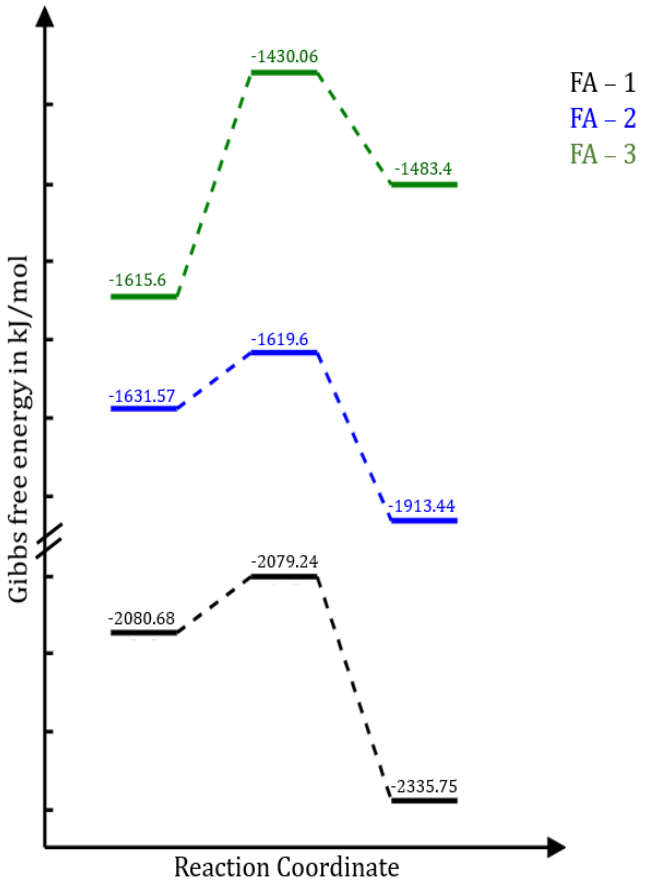

Fig. 19 Gibbs free energy plots of FA formation reactions at 298.15K. *(Scale modified for clarity.)*

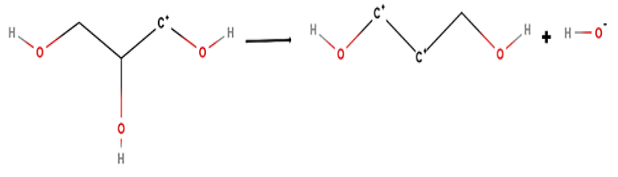

Fig. 20 $C_3H_6O_2$ formation from $C_3H_7O_3$.

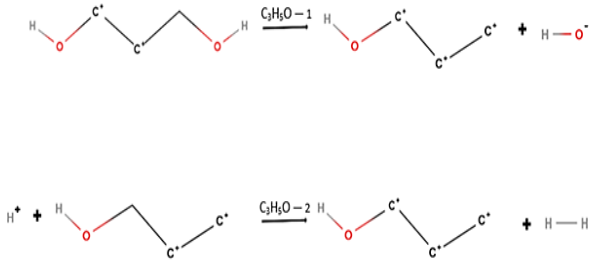

Fig. 21 C_3H_5O formation from $C_3H_6O_2$ and PA in C_3H_5O—1 and C_3H_5O—2 respectively.

3.4.3 Other observations

From the annealing simulations, which spanned a longer time and exhibited a thorough temperature regime, further reactions resulting in longer-chained species, were observed, such as methacrolein, crotonaldehyde, and pentanal as shown in Figs. 25-27. Since ChemTraYzer observed elementary steps, the species formed contain unpaired valence electrons.

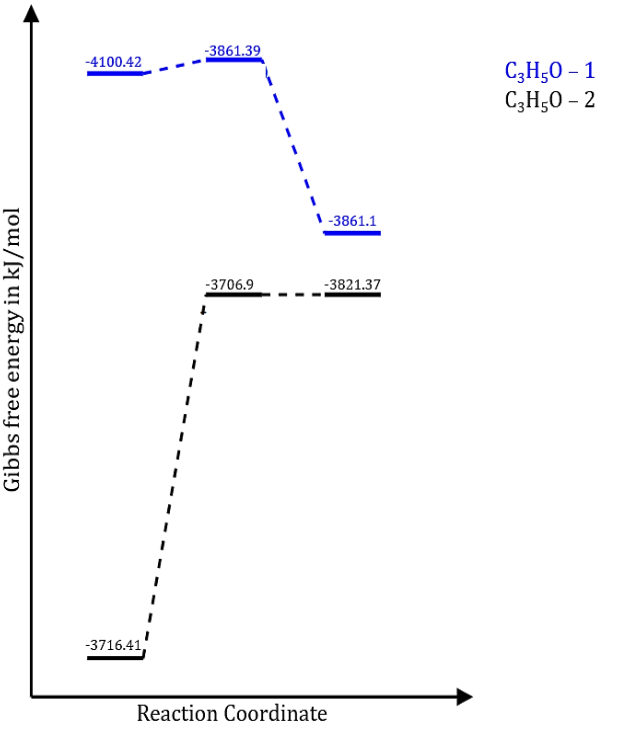

Fig. 22 Gibbs free energy plots of C_3H_5O formation reactions at 298.15K.

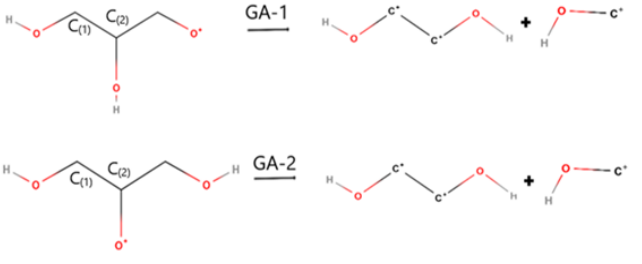

Fig. 23 GA formation from different configurations of $C_3H_7O_3$.

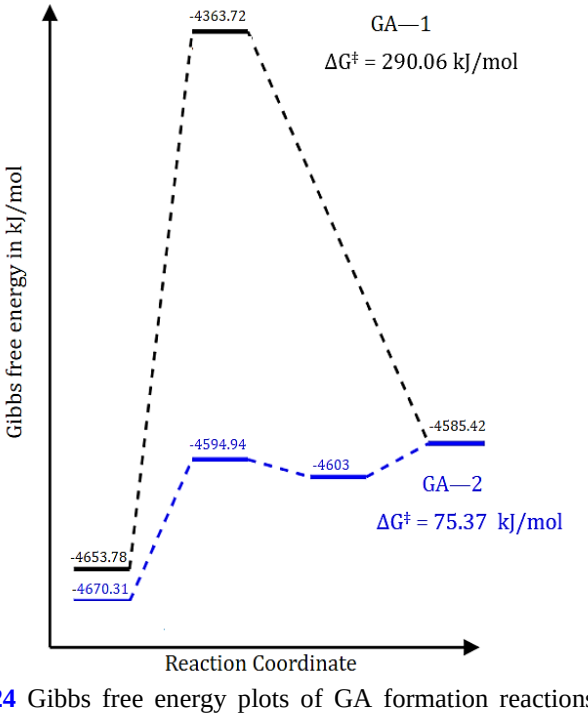

Fig. 24 Gibbs free energy plots of GA formation reactions at 298.15K.

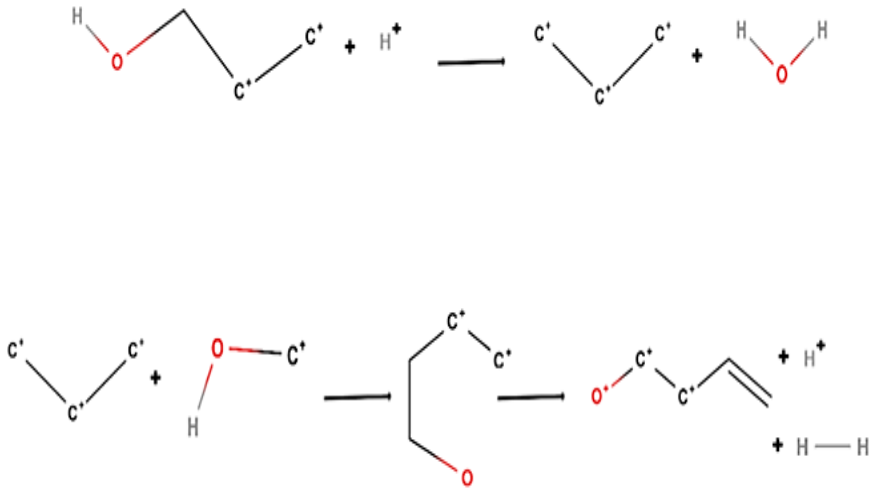

Fig. 25 Methacrolein formation two-step mechanism from C_3H_6O.

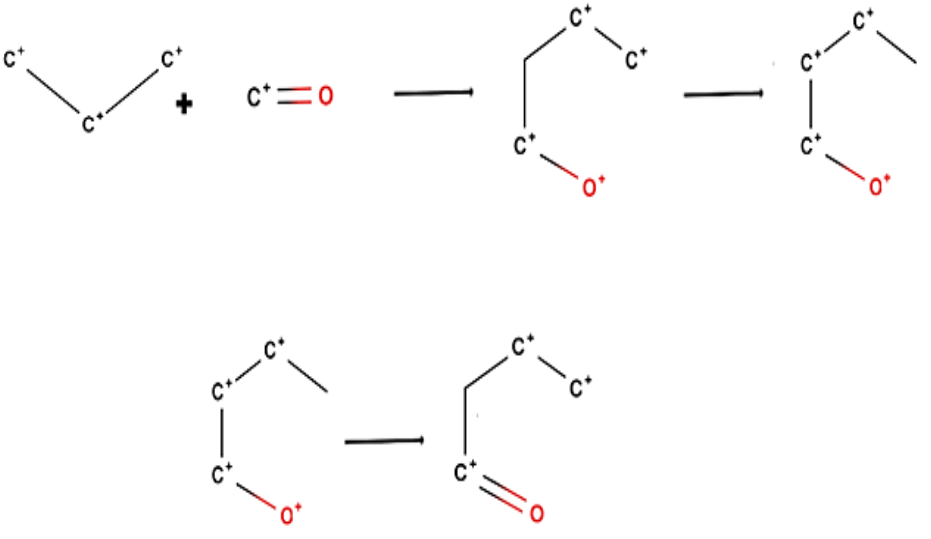

Fig. 26 Crotonaldehyde formation three-step mechanism from C_3H_5 and CHO.

In addition, aromatic compounds which were presented in some literature data on VG as an e-liquid,[11] were rarely detected in ChemTraYzer. The fact is, cyclical hydrocarbons, notably benzene and ethylbenzene, were formed at high density, ρ_3, annealing simulations with longer time steps (1000ps for the isothermal stage). Even at such conditions, they were not always detected. This is expected as, (1) benzene detection is more prominent with the presence of benzoic acid [37] and, (2) benzene formation in glycerol environments requires numerous chain reactions that could simply exceed the scope of our simulations [11] In fact, benzene detection in VG decomposition alone is lower than that of VG/benzoic acid systems as seen in Pankow *et al*. where the addition of benzoic acid to e-liquids significantly increased the detected benzene concentration.[37]

Nonetheless, the precursor for the formation of benzene and other aromatic compounds is acrolein.[11] The latter did form in our simulations, and underwent C—C cleavage to form ethylene free radical and FA as seen in Fig. 28.

The overall reaction pathway of VG degradation to the predominant products is presented in Fig. 29.

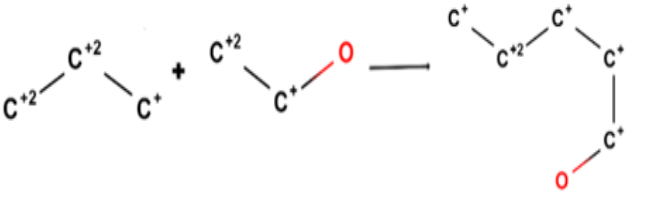

Fig. 27 Pentanal formation mechanism from C_3H_3 and C_2H_3O.

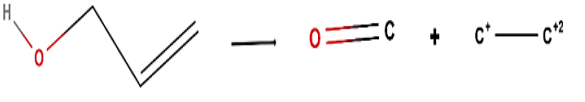

Fig. 28 Benzene pre-cursor reaction as detected by ChemTraYzer.

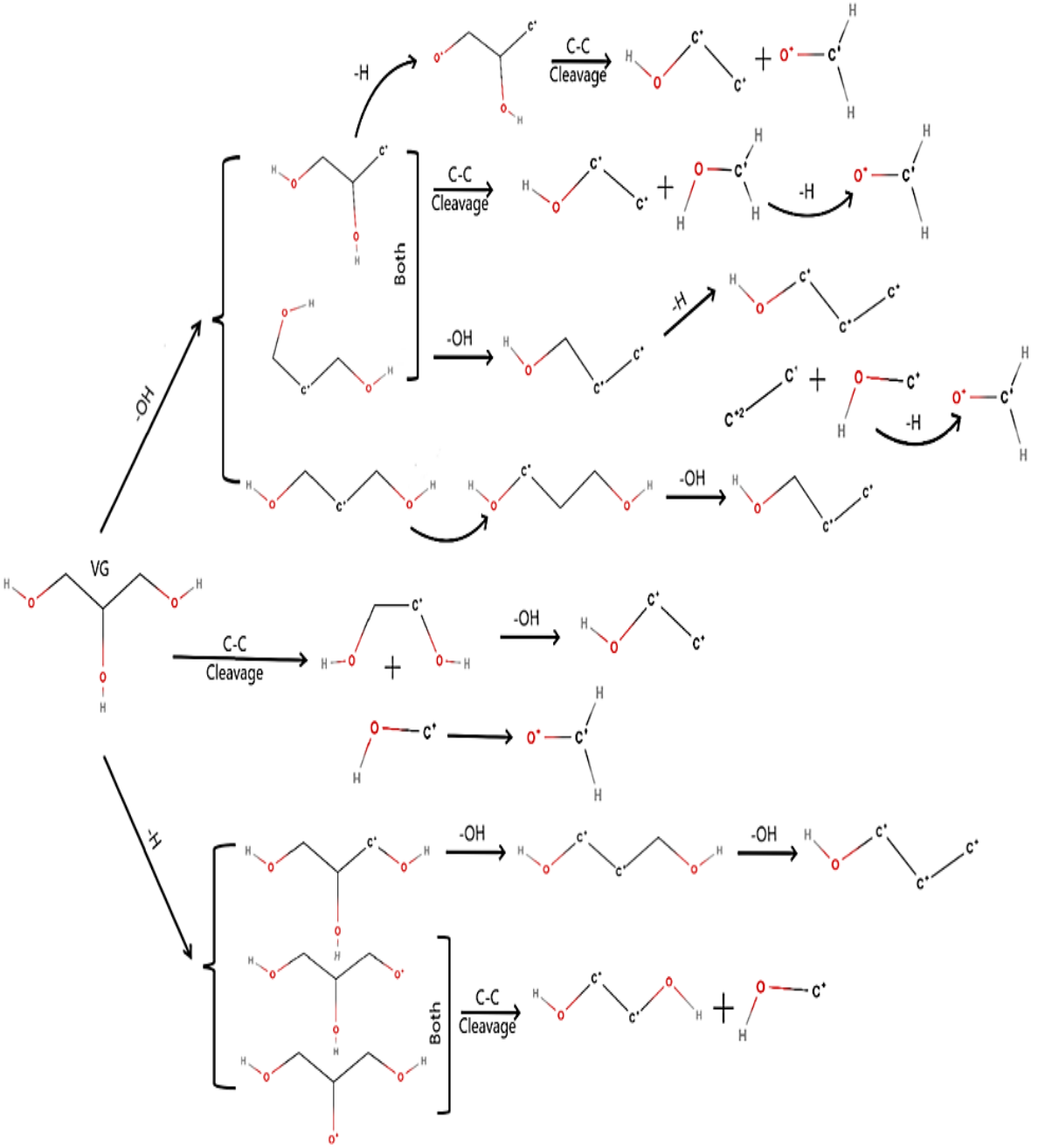

Fig. 29 VG overall decomposition pathways to main species.

4. Conclusion

The pyrolysis of VG was investigated in ReaxFF via molecular dynamics and transition state search. VG decomposition is composed of three main stages: the initial cracking of the VG molecule, the secondary reactions of cracking products into smaller-chained carbonyls, and the tertiary reactions where longer-chained and aromatic carbonyls are formed. From MD simulations, the rates of the overall VG decomposition and the formation reactions of notable species were found, with FA and AA being the dominant products. At a density of 0.13 g/mL, the activation energy of VG decomposition was 204.3 kJ/mol with a pre-exponential factor of 1.42E+14 s^{-1}. A detailed mechanism was presented for all three stages of VG decomposition, and the Gibbs free energy analyzed for the main reaction pathways. Pathway E, the loss of the middle hydroxyl group, exhibited the lowest activation energy at $\Delta G^{\ddagger} = 259.97$ *kJ/mol*, resulting eventually in the formation of FA and AA. VG decomposition depends closely on temperature as it is a thermal decomposition as seen in our temperature sensitivity study. From density sensitivity, it was seen that generally, the results (concentration profiles, Arrhenius parameters) became consistent at densities above 0.13 g/mL. The work herein presented a novel approach in thoroughly analyzing VG pyrolysis and its decomposition products.

Acknowledgments

This work was supported by the National Institute on Drug

Abuse of the National Institutes of Health (NIH grant number P50DA036105) and the Center for Tobacco Products of the U.S. Food and Drug Administration (FDA). The content is solely the responsibility of the authors and does not necessarily represent the official views of NIH or FDA.

Conflict of Interest

There is no conflict of interest.

Supporting Information

Not applicable.

References

[1] K. A. Wurzel, Glycerol. Encyclopedia of Toxicology (Second edition). Amsterdam: *Elsevier*, 2005, 449-451, doi: 10.1016/b0-12-369400-0/00457-9.

[2] M. N. N. Shahirah, J. Gimbun, A. Ideris, M. R. Khan, C. K. Cheng, Catalytic pyrolysis of glycerol into syngas over ceria-promoted Ni/α-Al_2O_3 catalyst, *Renewable Energy*, 2017, **107**, 223-234, doi: 10.1016/j.renene.2017.02.002.

[3] I. Hassan Al-Haj, Recent Advances in Pyrolysis, IntechOpen, Rijeka, 2020, doi: 10.5772/intechopen.77528.

[4] M. V. Singh, Pyrolysis of waste polyolefins into liquid petrochemicals using metal carbonate catalyst, *Engineered Science*, 2022, **19**, 285-291, doi: 10.30919/es8d699.

[5] T. Valliyappan, N. N. Bakhshi, A. K. Dalai, Pyrolysis of glycerol for the production of hydrogen or syn gas, *Bioresource Technology*, 2008, **99**, 4476-4483, doi: 10.1016/j.biortech.2007.08.069.

[6] A. Breland, E. Soule, A. Lopez, C. Ramôa, A. El-Hellani, T. Eissenberg, Electronic cigarettes: what are they and what do they do? *Annals of the New York Academy of Sciences*, 2017, **1394**, 5-30, doi: 10.1111/nyas.12977.

[7] N. A. Saliba, A. El Hellani, E. Honein, R. Salman, S. Talih, J. Zeaiter, A. Shihadeh, Surface chemistry of electronic cigarette electrical heating coils: effects of metal type on propylene glycol thermal decomposition, *Journal of Analytical and Applied Pyrolysis*, 2018, **134**, 520-525, doi: 10.1016/j.jaap.2018.07.019.

[8] C. AlGemayel, E. Honein, A. El Hellani, R. Salman, N. A. Saliba, A. Shihadeh, J. Zeaiter, Kinetic modeling of the pyrolysis of propylene glycol, *Engineered Science*, 2022, **20**, 162-179, doi: 10.30919/es8d757.

[9] N. R. Jaegers, W. Hu, T. J. Weber, J. Z. Hu, Low-temperature (< 200 °C) degradation of electronic nicotine delivery system liquids generates toxic aldehydes, *Scientific Reports*, 2021, **11**, 7800, doi: 10.1038/s41598-021-87044-x.

[10] R. P. Jensen, R. M. Strongin, D. H. Peyton, Solvent chemistry in the electronic cigarette reaction vessel, *Scientific Reports*, 2017, **7**, 42549, doi: 10.1038/srep42549.

[11] B. G. Ooi, D. Dutta, K. Kazipeta, N. S. Chong, Influence of the E-cigarette emission profile by the ratio of glycerol to propylene glycol in E-liquid composition, *ACS Omega*, 2019, **4**, 13338-13348, doi: 10.1021/acsomega.9b01504.

[12] R. M. Strongin, E-Cigarette chemistry and analytical detection, *Annual Review of Analytical Chemistry*, 2019, **12**, 23-39, doi: 10.1146/annurev-anchem-061318-115329.

[13] P. Wang, W. Chen, J. Liao,T. Matsuo, K. Ito, J. Fowles, D. Shusterman, M. Mendell, K. Kumagai, A device-independent evaluation of carbonyl emissions from heated electronic cigarette solvents, *PLOS ONE*, 2017, **12**, e0169811, doi: 10.1371/journal.pone.0169811.

[14] I. G. Gillman, K. A. Kistler, E. W. Stewart, A. R. Paolantonio, Effect of variable power levels on the yield of total aerosol mass and formation of aldehydes in e-cigarette aerosols, *Regulatory Toxicology and Pharmacology*, 2016, **75**, 58-65, doi: 10.1016/j.yrtph.2015.12.019.

[15] M. A. El Mubarak, C. Danika, N. S. Vlachos, K. Farsalinos, K. Poulas, G. Sivolapenko, Development and validation of analytical methodology for the quantification of aldehydes in e-cigarette aerosols using UHPLC-UV, *Food and Chemical Toxicology*, 2018, **116**, 147-151, doi: 10.1016/j.fct.2018.04.021.

[16] K. E. Farsalinos, K. A. Kistler, A. Pennington, A. Spyrou, D. Kouretas, G. Gillman, Aldehyde levels in e-cigarette aerosol: findings from a replication study and from use of a new-generation device, *Food and Chemical Toxicology*, 2018, **111**, 64-70, doi: 10.1016/j.fct.2017.11.002.

[17] K. E. Farsalinos, V. Voudris, K. Poulas, E-cigarettes generate high levels of aldehydes only in 'dry puff' conditions, *Addiction*, 2015, **110**, 1352-1356, doi: 10.1111/add.12942.

[18] Y. Fernández, A. Arenillas, M. A. Díez, J. J. Pis, J. A. Menéndez, Pyrolysis of glycerol over activated carbons for syngas production, *Journal of Analytical and Applied Pyrolysis*, 2009, **84**, 145-150, doi: 10.1016/j.jaap.2009.01.004.

[19] D. de OliveiraMaia, A. M. de SouzaChagas, A. M. de Morais Araújo, A. V. de Mendonça, I. M. de Lima Ferreira, F. C. D. Lemos, A. S. Araujo, V. J. Fernandes, A. D. Gondim, Catalytic pyrolysis of glycerol in the presence of Nickel (II) Schiff base complex supported in SBA-15: kinetic and products (TG-FTIR and PY-CG/MS), *Thermochimica Acta*, 2018, **669**, 160-168, doi: 10.1016/j.tca.2018.09.005.

[20] J. Piskorz, D. Radlein, D. S. Scott, On the mechanism of the rapid pyrolysis of cellulose, *Journal of Analytical and Applied Pyrolysis*, 1986, **9**, 121-137, doi: 10.1016/0165-2370(86)85003-3.

[21] Z. Geng, M. Zhang, Y. Yu, Theoretical investigation on pyrolysis mechanism of glycerol, *Fuel*, 2012, **93**, 92-98, doi: 10.1016/j.fuel.2011.08.021.

[22] D. Zhang, Y. Cao, P. Zhang, J. Liang, K. Xue, Y. Xia, Z. Qi, Investigation of the thermal decomposition mechanism of glycerol: the combination of a theoretical study based on the Minnesota functional and experimental support, *Physical Chemistry Chemical Physics*, 2021, **23**, 20466-20477, doi: 10.1039/d1cp01526e.

[23] T. Laino, C. Tuma, A. Curioni, E. Jochnowitz, S. Stolz, A revisited picture of the mechanism of glycerol dehydration, *The Journal of Physical Chemistry A*, 2011, **115**, 3592-3595, doi: 10.1021/jp201078e.

[24] ReaxFF: reactive MD with graphical interface & analysis

tools Software for Chemistry & Materials, Software for Chemistry and Materials, 2022, https://www.scm.com/product/reaxff/.
[25] A. C. T. van Duin, S. Dasgupta, F. Lorant, W. A. Goddard, ReaxFF: A reactive force field for hydrocarbons, *The Journal of Physical Chemistry A*, 2001, **105**, 9396-9409, doi: 10.1021/jp004368u.
[26] L. Martínez, R. Andrade, E. G. Birgin, J. M. Martínez, PACKMOL: A package for building initial configurations for molecular dynamics simulations, *Journal of Computational Chemistry*, 2009, **30**, 2157-2164, doi: 10.1002/jcc.21224
[27] S. Arvelos, O. Abrahão Jr, C. Eponina Hori, ReaxFF molecular dynamics study on the pyrolysis process of cyclohexanone, *Journal of Analytical and Applied Pyrolysis*, 2019, **141**, 104620, doi: 10.1016/j.jaap.2019.05.009.
[28] Q.-D. Wang, J.-B. Wang, J.-Q. Li, N.-X. Tan, X.-Y. Li, Reactive molecular dynamics simulation and chemical kinetic modeling of pyrolysis and combustion of n-dodecane, *Combustion and Flame*, 2011, **158**, 217-226, doi: 10.1016/j.combustflame.2010.08.010.
[29] T. Zhao, T. Li, Z. Xin, L. Zou, L. Zhang, A ReaxFF-based molecular dynamics simulation of the pyrolysis mechanism for polycarbonate, *Energy & Fuels*, 2018, **32**, 2156-2162, doi: 10.1021/acs.energyfuels.7b03332.
[30] Z. Chen, W. Sun, L. Zhao, High-temperature and high-pressure pyrolysis of hexadecane: molecular dynamic simulation based on reactive force field (ReaxFF), *The Journal of Physical Chemistry A*, 2017, **121**, 2069-2078, 10.1021/acs.jpca.6b12367.
[31] Y. Wang, S. Gong, H. Wang, L. Li, G. Liu, High-temperature pyrolysis of isoprenoid hydrocarbon p-menthane using ReaxFF molecular dynamics simulation, *Journal of Analytical and Applied Pyrolysis*, 2021, **155**, 105045, doi: 10.1016/j.jaap.2021.105045.
[32] A. Lele, H. Kwon, K. Ganeshan, Y. Xuan, A. C. T. van Duin, ReaxFF molecular dynamics study on pyrolysis of bicyclic compounds for aviation fuel, *Fuel*, 2021, **297**, 120724, doi: 10.1016/j.fuel.2021.120724.
[33] S. Yan, D. Xia, W. Xuan, New insight into enhancement effect of supercritical water on scrap tire depolymerization: a study based on ReaxFF-MD simulation and DFT method, *Fuel Processing Technology*, 2020, **200**, 106309, doi: 10.1016/j.fuproc.2019.106309.
[34] Y. Qian, W. Xu, J.-H. Zhan, X. Jia, F. Zhang, Atomic insights into the thermal runaway process of hydrogen peroxide and 1, 3, 5-trimethybenzene mixture: combining ReaxFF MD and DFT methods, *Process Safety and Environmental Protection*, 2021, **147**, 578-588, doi: 10.1016/j.psep.2020.12.036.
[35] D. G. Truhlar, in Encyclopedia of Physical Science and Technology, (Third Edition), R. A. Meyers, Ed. Academic Press, New York, 2003, 9-17.
[36] P. W. Atkins, J. De Paula, Atkins Physical Chemistry, Physical chemistry Oxford University Press, Oxford, ed. 10th, 2014.
[37] J. F. Pankow, K. Kim, K. J. McWhirter, W. Luo, J. O. Escobedo, R. M. Strongin, A. K. Duell, D. H. Peyton, Benzene formation in electronic cigarettes, *PLoS One*, 2017, **12**, e0173055, doi: 10.1371/journal.pone.0173055.

